








# Calibrating the *James Webb Space Telescope* Filters as Star Formation Rate Indicators

Madhooshi R. Senarath<sup>1,2</sup> , Michael J. I. Brown<sup>1,2</sup> , Michelle E. Cluver<sup>3,4</sup> , John Moustakas<sup>5</sup>,  
Lee Armus<sup>6</sup> , and Thomas H. Jarrett<sup>7</sup> 

<sup>1</sup> School of Physics and Astronomy, Monash University, Clayton, VIC 3800, Australia; [madhooshi.senarath@monash.edu](mailto:madhooshi.senarath@monash.edu)

<sup>2</sup> Monash Centre for Astrophysics, Monash University, Clayton, VIC 3800, Australia

<sup>3</sup> Centre for Astrophysics and Supercomputing, Swinburne University of Technology, Hawthorne, VIC 3122, Australia

<sup>4</sup> Department of Physics and Astronomy, University of the Western Cape, Robert Sobukwe Road, Bellville, 7535, South Africa

<sup>5</sup> Department of Physics and Astronomy, Siena College, 515 Loudon Road, Loudonville, NY 12211, USA

<sup>6</sup> IPAC, California Institute of Technology, Pasadena, CA 91125, USA

<sup>7</sup> Department of Astronomy, University of Cape Town, Private Bag X3, Rondebosch, 7701, South Africa

Received 2018 September 25; revised 2018 November 28; accepted 2018 November 28; published 2018 December 14

## Abstract

We have calibrated the 6.5 m *James Webb Space Telescope* (*JWST*) mid-infrared (MIR) filters as star formation rate (SFR) indicators, using *JWST* photometry synthesized from *Spitzer* spectra of 49 low-redshift galaxies, which cover a wider luminosity range than most previous studies. We use Balmer-decrement-corrected  $H\alpha$  luminosity and synthesized MIR photometry to empirically calibrate the *Spitzer*, *WISE*, and *JWST* filters as SFR indicators. Our *Spitzer* and *WISE* calibrations are in good agreement with recent calibrations from the literature. While MIR luminosity may be directly proportional to SFR for high-luminosity galaxies, we find a power-law relationship between MIR luminosity and SFR for low-luminosity galaxies ( $L_{H\alpha} \leq 10^{43}$  erg s<sup>-1</sup>). We find that for galaxies with an  $H\alpha$  luminosity of  $10^{40}$  erg s<sup>-1</sup> (corresponding to an SFR of  $\sim 0.055 M_{\odot}$  yr<sup>-1</sup>), the corresponding *JWST* MIR  $\nu L_{\nu}$  luminosity is between  $10^{40.50}$  and  $10^{41.00}$  erg s<sup>-1</sup>. Power-law fits of *JWST* luminosity as a function of  $H\alpha$  luminosity have indices between 1.17 and 1.32. We find that the scatter in the *JWST* filter calibrations decreases with increasing wavelength from 0.39 to 0.20 dex, although F1000W is an exception where the scatter is just 0.24 dex.

**Key words:** galaxies: evolution – galaxies: general – galaxies: photometry – stars: formation

## 1. Introduction

Galaxies grow via both star formation and galaxy mergers, so star formation rate (SFR) measurements are crucial for understanding galaxy evolution. SFR measurements can utilize spectra and imaging of both emission lines and continuum, and include (but are not limited to) line emission from  $H\alpha$  and Pa $\alpha$  and continuum emission in the ultraviolet (UV), infrared (IR), and radio. These wavebands trace the presence or recent death of high-mass stars with short lifetimes ( $\lesssim 100$  Myr; e.g., Kennicutt 1998; Kennicutt & Evans 2012; Davies et al. 2015 and references therein). UV and  $H\alpha$  luminosities as a function of SFR can be predicted from theory (e.g., Kennicutt 1998, and references therein), but both can suffer greatly from dust attenuation, which can result in large uncertainties and systematics in measured SFRs. Mid-infrared (MIR) emission from dust and polycyclic aromatic hydrocarbons (PAHs) associated with star formation suffers little from dust obscuration, making it a potentially powerful SFR indicator. The main contaminant in MIR SFR calibrations is dust heated by old stellar populations that are unassociated with recent star formation, although the significance of this effect becomes less important for shorter MIR wavelengths (e.g., Calzetti et al. 2010; Kennicutt & Evans 2012). Critically, MIR SFR indicators require empirical calibration.

The 6.5 m *James Webb Space Telescope* (*JWST*), will be the most sensitive MIR telescope built to date, and will be able to measure SFRs for galaxies at  $z < 3$ . *JWST*'s Mid-Infrared Instrument (MIRI) spans wavelengths between 5 and 30  $\mu\text{m}$  using nine filters with effective wavelengths of 5.6, 7.7, 10, 11.3, 12.8, 15, 18, 21, and 25.5  $\mu\text{m}$  (Bouchet et al. 2015). For point sources with exposure times of  $10^4$  s, *JWST* has a sensitivity of  $\sim 10^{-6}$  Jy for 8–30  $\mu\text{m}$  (signal-to-noise ratio of

10), far deeper than *Spitzer* and *WISE*, which have sensitivities  $\sim 10^{-5}$  Jy and  $\sim 10^{-3}$  Jy, respectively (Glasse et al. 2015).

In this Letter we calibrate the *JWST* MIR filters as SFR indicators. As *JWST* has yet to be launched, we calibrate the *JWST* MIR filters using photometry synthesized from *Spitzer* spectra of low-redshift galaxies (Brown et al. 2014, 2017). To validate our approach, we also calibrate the *Spitzer* and *WISE* MIR filters using the same methods and spectra, enabling direct comparison with prior literature. Battisti et al. (2015) have also calibrated six MIRI filters using a sample of high-luminosity galaxies with SFRs of  $\sim 1$ – $10 M_{\odot}$  yr<sup>-1</sup>, whereas our calibrations are made using lower-luminosity galaxies that cover a wider luminosity range.

Throughout this Letter we use AB magnitudes, and a Hubble constant of  $H_0 = 71.9$  km s<sup>-1</sup> Mpc<sup>-1</sup> (Bonvin et al. 2017). We also adopt a Kroupa (2001)<sup>8</sup> initial mass function (IMF) for this Letter, where we use the Kennicutt et al. (2009) conversion from  $L_{H\alpha, \text{corr}}$  to SFR for a Kroupa (2001) IMF. Throughout this Letter we use  $\nu L_{\nu}$  luminosities in units of erg s<sup>-1</sup>, which is consistent with several recent SFR calibration papers (e.g., Kennicutt et al. 2009; Jarrett et al. 2011; Battisti et al. 2015; Brown et al. 2017; Cluver et al. 2017).

## 2. Sample Selection and Emission Line Measurements

To calibrate MIR SFR indicators, we need a sample of galaxies with accurate MIR luminosities and accurate measurements of an SFR indicator that can be calibrated from theory

<sup>8</sup> In this Letter we convert from  $L_{H\alpha, \text{corr}}$  to SFR using:  $\text{SFR}(M_{\odot} \text{ yr}^{-1}) = 5.5 \times 10^{-42} L_{H\alpha}(\text{erg s}^{-1})$  for a Kroupa (2001; Kennicutt et al. 2009). To convert from Salpeter (1955) IMF and Chabrier (2003) IMF to Kroupa (2001) IMF, the multiplicative factor is 0.70 and 1.20, respectively (Kennicutt et al. 2009; Jaskot et al. 2015).

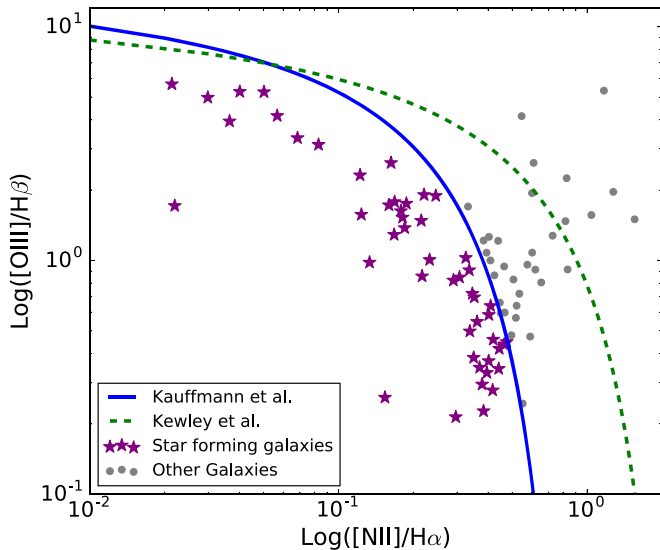


**Figure 1.** BPT diagram of the 82 galaxies from Brown et al. (2014) where the measured  $H\alpha$  and  $H\beta$  emission line fluxes have a signal-to-noise greater than five. We plot both the Kewley et al. (2001) and Kauffmann et al. (2003) criteria, and use the Kauffmann et al. (2003) criterion as it rejects more potential AGNs and LINERS. This leaves 49 star-forming galaxies.

(i.e.,  $H\alpha$ , UV, and total infrared (TIR)). We use the Brown et al. (2014) galaxy spectra and accompanying optical emission-line measurements (Brown et al. 2017) to calibrate the *JWST* MIRI filters as SFR indicators. Brown et al. (2014) use matched aperture photometry to rescale the optical and MIR spectroscopy, thus mitigating aperture bias. The median rescale factors for our sample of 49 galaxies for *Spitzer* 8  $\mu\text{m}$ , 12  $\mu\text{m}$ , and 20  $\mu\text{m}$  filters are 1.50, 1.52, and 1.18 respectively, and at 8  $\mu\text{m}$  have a range of 0.88–4.70 (Brown et al. 2014). The sample galaxies are at redshifts of  $z < 0.05$  and have absolute magnitudes of  $-14.7 \geq M_g \geq -23.2$ . We refer the reader to Brown et al. (2014) for photometric data of the galaxies and to Appendix A of Brown et al. (2014) for the Infrared Spectrograph (IRS) spectra of the galaxies.

The optical emission line fluxes are taken from Brown et al. (2017), which utilize optical spectra first presented in Moustakas & Kennicutt (2006) and Moustakas et al. (2010). Following Moustakas et al. (2010), these revised emission line fluxes were determined using modified versions of pPXF (Cappellari & Emsellem 2004) and GANDALF<sup>9</sup> (Sarzi et al. 2006) to model the stellar continuum and emission lines, respectively. The Brown et al. (2014) sample contains 129 galaxies, but limiting this sample to those galaxies with nebular emission lines that satisfy a signal-to-noise threshold of five for  $H\alpha$  and  $H\beta$  reduces the sample to 82 galaxies.

To separate active galactic nuclei (AGNs) and low-ionization nuclear emission-line regions (LINERS) from star-forming galaxies, we use the Baldwin, Phillips, and Terlevich (BPT; Baldwin et al. 1981) diagnostic diagram. Figure 1 shows the BPT diagram for our sample, along with the Kewley et al. (2001) and Kauffmann et al. (2003) criteria for selecting star-forming galaxies. We have used the empirical Kauffmann et al. (2003) criterion as it is more conservative, rejecting more galaxies that could potentially be AGNs or LINERS than

Kewley et al. (2001). This reduces our sample size from 82 galaxies to 49 star-forming galaxies.

Our SFR calibrations are anchored to  $H\alpha$  luminosities, which must be corrected for dust extinction. We used the extinction law of Cardelli et al. (1989) for nebular emission and the Calzetti et al. (2000) starburst attenuation curve for the stellar continuum (although we do not use the dust corrected stellar continuum in this particular Letter). We adopt the intrinsic emission line flux ratios of Osterbrock (1989) for Case B recombination with an effective temperature of 10,000 K and electron density of  $n_e = 10^2 \text{ cm}^{-3}$ , giving an  $H\alpha$  to  $H\beta$  ratio of 2.86.

### 3. *JWST* Photometry

As *JWST* has yet to be launched and take observations, our SFR calibrations rely on photometry that we have synthesized from *Spitzer* MIR spectroscopy of nearby galaxies (Brown et al. 2014). As Brown et al. (2014) includes MIR spectroscopy from *Spitzer* and MIR photometry from *Spitzer* and *WISE*, we can validate our approach by determining new SFR calibrations for *Spitzer* and *WISE* with synthesized photometry and directly comparing them to the Brown et al. (2017) calibrations that used directly measured photometry. Galaxy luminosities are determined using (synthesized) apparent magnitudes and distances, with redshift-independent distances being used when available (all taken from the compilation of Brown et al. 2017). It should be noted that our sample has considerable overlap with that of Brown et al. (2017), but does not include the Brown et al. (2017) galaxies that do not have *Spitzer* MIR spectroscopy.

Synthetic apparent magnitudes were determined using

$$m = -2.5 \log \left[ \left( \int R(\nu) \frac{f_\nu(\nu)}{h\nu} d\nu \right) \times \left( \int R(\nu) \frac{g_\nu(\nu)}{h\nu} d\nu \right)^{-1} \right] \quad (1)$$

where  $R(\nu)$  is the filter response function (electrons per incident photon),  $h\nu$  is the energy of a photon with frequency  $\nu$ ,  $f_\nu$  is the galaxy spectral energy distribution (SED) and  $g_\nu(\nu)$  is an AB magnitude zero source, with a flux density of 3631 Jy (e.g., Hogg et al. 2002).

For SFRs measured using photometry, it is common to use  $f_\nu$  and  $L_\nu$  defined using the apparent magnitude and the effective wavelength of the filter. This definition differs from Equation (1), and is given by

$$f_\nu = 3631 \text{ Jy} \times 10^{-0.4m} \quad (2)$$

where the  $m$  is the apparent magnitude. For *JWST* we use the effective wavelengths defined by Bouchet et al. (2015), while for *Spitzer* and *WISE* we use the effective wavelengths provided by Brown et al. (2017).

To summarize the properties of our sample and for comparisons to prior literature, in Figure 2 we show a color-color diagram derived using MIRI and NIRcam filter curves (Greene et al. 2017), which is similar to the *WISE* color-color diagram of Jarrett et al. (2011). We used all 129 galaxies from Brown et al. (2014) plus 16 additional AGN spectra from M. J. I. Brown et al. (2019, in preparation).

<sup>9</sup> Gas and Absorption Line Fitting Algorithm (Falcon-Barroso et al. 2006; Sarzi et al. 2006).

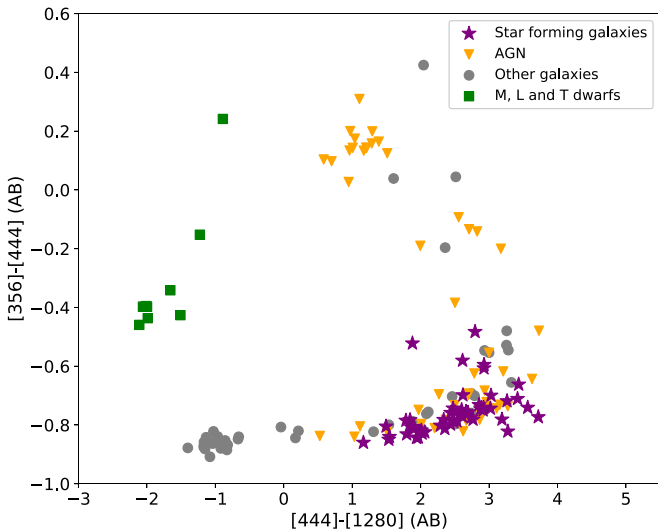


**Figure 2.** *JWST* NIRcam and MIRI color-color diagram. The AGNs in this figure are BPT-selected AGNs from Brown et al. (2014) and quasars (M. J. I. Brown et al. 2019, in preparation), including AGNs dominated by host galaxy light that have MIR colors similar to star-forming galaxies. Our diagram is similar to the *WISE* color-color diagram of Jarrett et al. (2011), as we have used filters with comparable effective wavelengths, and illustrates how MIR can separate powerful AGNs, passive galaxies, MLT dwarfs, and star-forming galaxies.

New infrared SEDs for brown dwarfs and quasars were created by combining archival *Akari* and *Spitzer* spectra.<sup>10,11</sup> These were selected under the conditions that the spectra of a specific object appear in both archives and the *Spitzer* and *Akari* spectra had consistent flux densities at  $\sim 5 \mu\text{m}$ . Unsurprisingly, the *JWST* color-color diagram closely resembles the *WISE* color-color diagram and illustrates the (well-known) utility of MIR photometry to select passive galaxies, star-forming galaxies, brown dwarfs, and quasars. A complete discussion of *JWST* color selection of different types of celestial object is beyond the scope of this Letter, but will be expanded on in a future work.

#### 4. MIR Filter Calibrations

To validate the methods we use to calibrate the *JWST* MIRI filters, we first calibrate the *WISE*, *Spitzer* IRAC, and *Spitzer* MIPS  $24 \mu\text{m}$  MIR filters using photometry synthesized from the Brown et al. (2014) spectra. These filters have been previously calibrated in the prior literature, which allows us to cross-check our methodology.

To calibrate a specific wavelength (or filter) as an SFR indicator, we model the relationship between the luminosity (at the relevant wavelength) and Balmer-decrement-corrected  $L_{\text{H}\alpha}$  ( $L_{\text{H}\alpha, \text{corr}}$ ). We used the least squares method to do this, which assumed a Gaussian scatter of the data about the line of best fit. The relationship between  $\text{H}\alpha$  luminosity and MIR luminosity is often modeled with a power law (e.g., Wu et al. 2005; Zhu et al. 2008; Kennicutt et al. 2009; Jarrett et al. 2013; Lee et al. 2013; Brown et al. 2014, 2017; Cluver et al. 2014, 2017;

Battisti et al. 2015, and references therein), and thus we also use this parameterization.

As illustrated in Figure 3 and Table 1, for galaxies with a  $\text{H}\alpha$  luminosity of  $10^{40} \text{ erg s}^{-1}$ , we find the corresponding *WISE* and *Spitzer*  $\nu L_\nu$  is between  $10^{40.49}$  and  $10^{41.37} \text{ erg s}^{-1}$ . We find that the relationship between MIR luminosity and SFR is a power law with indices in the range of 1.22–1.31. The *WISE* W4 normalizations and power-law indices agree to within 0.11 and 0.04 dex, respectively, of the Brown et al. (2017) estimates. Our *Spitzer* normalizations and power-law indices agree to within 0.08 and 0.08 dex, respectively, of the Brown et al. (2017) estimates. These agreements build confidence in our methods, and their utilization for the *JWST* MIRI filters. Brown et al. (2017) included a number of dwarf galaxies in their sample that do not have MIR spectroscopy (and are thus excluded from our study), and we believe this is the main reason for the small systematic difference between our fits and those of Brown et al. (2017), where we measure slightly smaller power-law indices. The dwarf galaxies extend to lower luminosities than covered by the sample that we use for our calibrations.

The power-law fits for *Spitzer* 5.8 and  $8 \mu\text{m}$  filters determined by other studies (e.g., Wu et al. 2005; Zhu et al. 2008) have smaller indices than those of Brown et al. (2017) fits and our fits. One reason for this discrepancy is that we cover a broader range of  $\text{H}\alpha$  luminosities than much of the prior literature, going down to  $10^{39} \text{ erg s}^{-1}$ . Some studies also adopt a power-law index of 1; however, dust content varies with galaxy mass (e.g., Calzetti et al. 2000), so this assumption is (at best) an approximation. For studies that use mostly high-luminosity galaxies, the power-law indices are noticeably shallower, and create discrepancies when extrapolated to low-luminosity dwarf galaxies (e.g., Wu et al. 2005; Kennicutt et al. 2009).

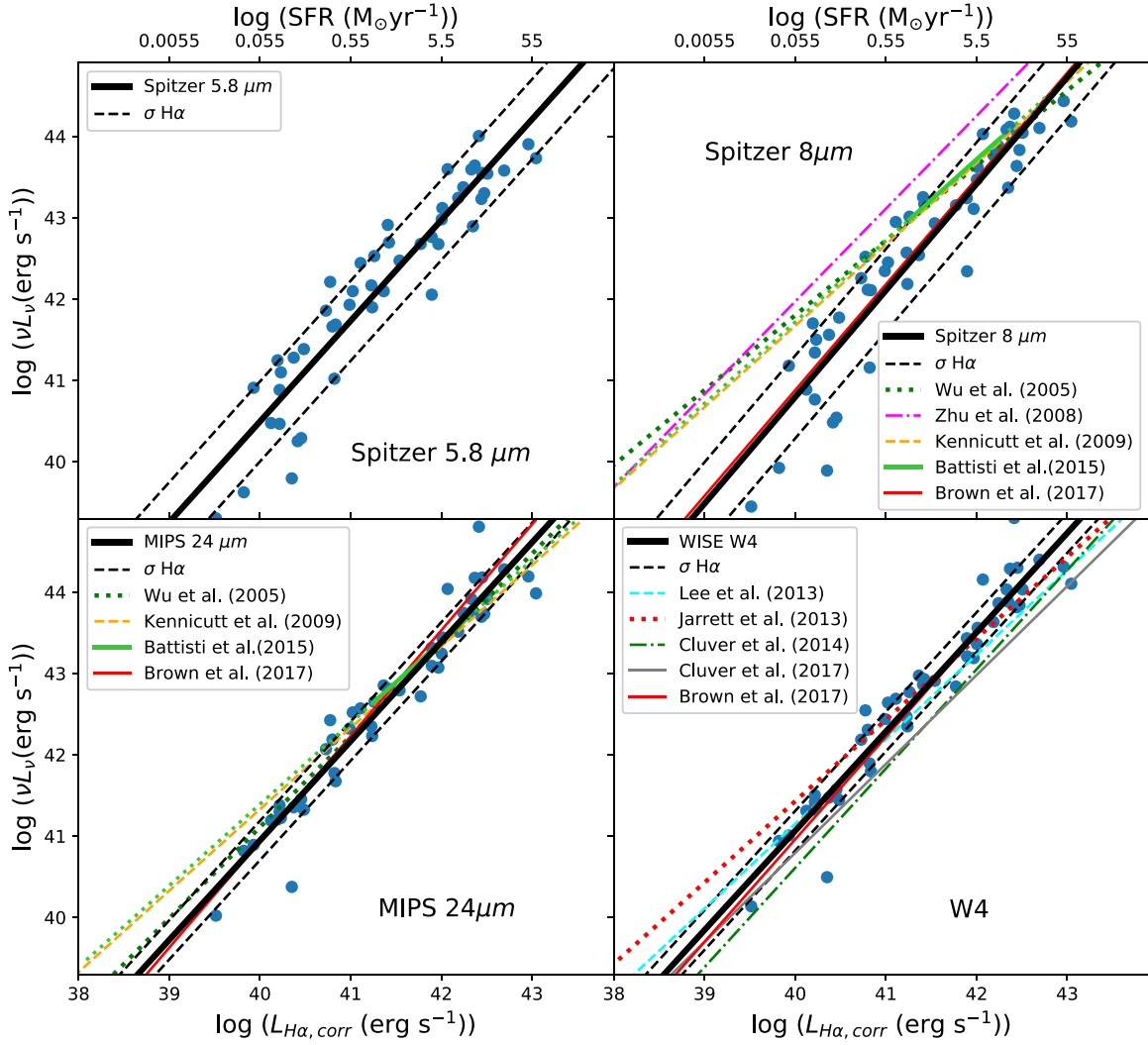
We used  $\chi^2$  statistics to determine the uncertainties of our fits of luminosity versus  $L_{\text{H}\alpha}$  relationship. The  $1\sigma$  scatter about the line of best fit was determined by finding the range above and below fit that encompassed 68% of the data. We present both the MIR scatter  $\sigma_{\nu L_\nu}$  and the  $L_{\text{H}\alpha}$  scatter,  $\sigma_{L_{\text{H}\alpha}}$ , with the latter providing an estimate of the accuracy of MIR measurements of star formation. Brown et al. (2017) also measured the  $1\sigma$  scatter about their calibration lines ( $\sigma_{L_{\text{H}\alpha}}$  and  $\sigma_{\nu L_\nu}$ ), and we measure comparable scatter to Brown et al. (2017) for our calibrations. It should be noted that the scatter in the power-law fit is dominated by the true scatter of galaxies about the best-fit relationship, rather than being dominated by random errors (i.e., distance errors and photometric uncertainties) or systematic errors (i.e., Hubble constant errors, filter curve errors, and zero point errors).

Figure 4 shows our SFR calibrations for six of the nine *JWST* MIRI filters. In Figure 4, we also plot our relations and those of Brown et al. (2017) for comparable *Spitzer* filters. We find good agreement for the F770W and F2550W filters with the normalizations and power-law indices agreeing within 0.05 dex and 0.01, respectively, of our *Spitzer* calibrations. This builds confidence in our measurements for these wavelengths as well as the other seven *JWST* MIRI filters.

For galaxies with a  $\text{H}\alpha$  luminosity of  $10^{40} \text{ erg s}^{-1}$ , the corresponding *JWST* MIRI  $\nu L_\nu$  luminosity is between  $10^{40.50}$  and  $10^{41.00} \text{ erg s}^{-1}$ . Power-law fits of the data have indices between 1.17 and 1.32. Normalization and power-law fits, their uncertainties, and scatter are all presented in Table 1.

<sup>10</sup> <http://cassis.sirtf.com/atlas/welcome.shtml> and <http://www.ir.isas.jaxa.jp>

<sup>11</sup> The archival spectra used in Figure 2 are GJ1111, epsIndBa+Bb, J0036+1821, LHS3003, vB10, G196-3A, BRI0021-0214, J042348-0414, GJ1001A, 3C 273, 3C 351, Mrk 509, Mrk 876, PG 0052+251, PG 1211+143, PG 1415+451, PG 2349-014, Ton 951, 3C 120, Ark 120, Mrk 110, Mrk 279, Mrk 290, Mrk 590, and Mrk 817.



**Figure 3.** Our *Spitzer* and *WISE* SFR calibrations, along with calibrations from previous literature for comparison (Wu et al. 2005; Zhu et al. 2008; Kennicutt et al. 2009; Lee et al. 2013; Jarrett et al. 2013; Cluver et al. 2014, 2017; Battisti et al. 2015; Brown et al. 2017). Our fits for *Spitzer* and *WISE* and the equivalents from Brown et al. (2017; shown in red) agree within each others' uncertainties, building confidence that our method can also be used for the *JWST* MIRI filters. The solid green line segments represent the MIRI calibrations of Battisti et al. (2015) for the relevant SFR range, with the dotted green lines then extrapolating to lower SFRs.

**Table 1**  
SFR Indicator Calibrations

Indicator	Fit to $\log(\nu L_\nu)$	$\sigma_{L_{H\alpha}}$ (dex)	$\sigma_{\nu L_\nu}$ (dex)	Effective Wavelength
<i>Spitzer</i> 5.8 $\mu\text{m}$	$(40.49 \pm 0.10) + (1.24 \pm 0.06) \times [\log(L_{H\alpha, \text{corr}}) - 40]$	0.40	0.49	5.73 $\mu\text{m}$
<i>Spitzer</i> 8 $\mu\text{m}$	$(40.80 \pm 0.11) + (1.31 \pm 0.08) \times [\log(L_{H\alpha, \text{corr}}) - 40]$	0.39	0.51	7.87 $\mu\text{m}$
<i>Spitzer</i> MIPS 24 $\mu\text{m}$	$(40.95 \pm 0.09) + (1.22 \pm 0.07) \times [\log(L_{H\alpha, \text{corr}}) - 40]$	0.20	0.24	23.68 $\mu\text{m}$
<i>WISE</i> W3	$(41.37 \pm 0.13) + (1.24 \pm 0.08) \times [\log(L_{H\alpha, \text{corr}}) - 40]$	0.31	0.38	11.56 $\mu\text{m}$
<i>WISE</i> W4	$(41.07 \pm 0.07) + (1.22 \pm 0.06) \times [\log(L_{H\alpha, \text{corr}}) - 40]$	0.20	0.24	22.8 $\mu\text{m}$
<i>JWST</i> F560W	$(40.50 \pm 0.09) + (1.22 \pm 0.08) \times [\log(L_{H\alpha, \text{corr}}) - 40]$	0.38	0.47	5.6 $\mu\text{m}$
<i>JWST</i> F770W	$(40.78 \pm 0.13) + (1.32 \pm 0.07) \times [\log(L_{H\alpha, \text{corr}}) - 40]$	0.39	0.52	7.7 $\mu\text{m}$
<i>JWST</i> F1000W	$(40.64 \pm 0.10) + (1.17 \pm 0.05) \times [\log(L_{H\alpha, \text{corr}}) - 40]$	0.24	0.28	10 $\mu\text{m}$
<i>JWST</i> F1130W	$(40.87 \pm 0.12) + (1.26 \pm 0.08) \times [\log(L_{H\alpha, \text{corr}}) - 40]$	0.30	0.37	11.3 $\mu\text{m}$
<i>JWST</i> F1280W	$(40.78 \pm 0.08) + (1.24 \pm 0.05) \times [\log(L_{H\alpha, \text{corr}}) - 40]$	0.30	0.37	12.8 $\mu\text{m}$
<i>JWST</i> F1500W	$(40.74 \pm 0.09) + (1.21 \pm 0.05) \times [\log(L_{H\alpha, \text{corr}}) - 40]$	0.24	0.29	15 $\mu\text{m}$
<i>JWST</i> F1800W	$(40.86 \pm 0.09) + (1.20 \pm 0.07) \times [\log(L_{H\alpha, \text{corr}}) - 40]$	0.24	0.29	18 $\mu\text{m}$
<i>JWST</i> F2100W	$(40.92 \pm 0.09) + (1.20 \pm 0.07) \times [\log(L_{H\alpha, \text{corr}}) - 40]$	0.21	0.25	21 $\mu\text{m}$
<i>JWST</i> F2550W	$(41.00 \pm 0.10) + (1.23 \pm 0.07) \times [\log(L_{H\alpha, \text{corr}}) - 40]$	0.20	0.24	25.5 $\mu\text{m}$

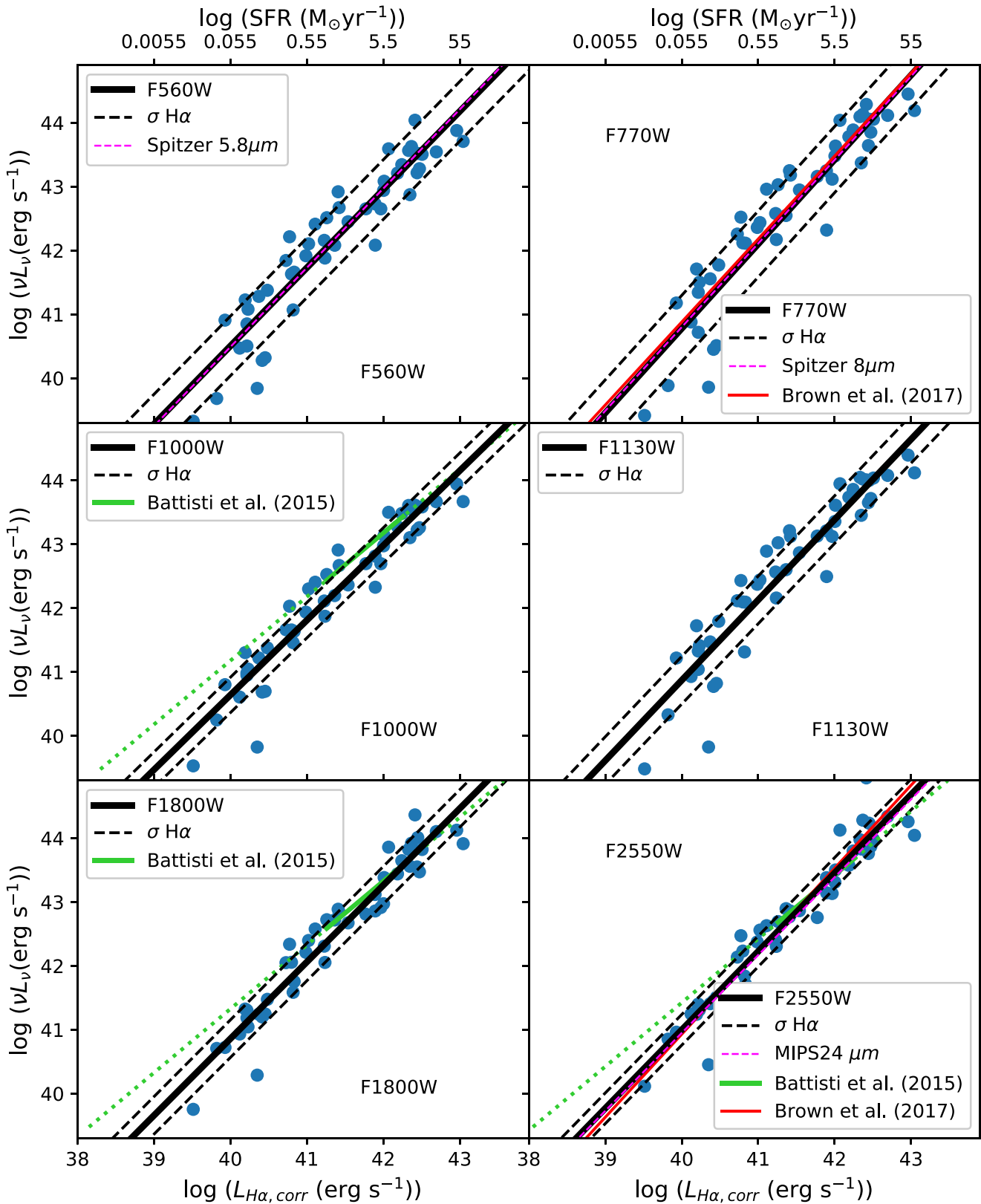


**Figure 4.** Calibrations of six out of the nine *JWST* MIRI filters. The black dashed lines in the individual plots enclose  $1\sigma$  of the SFR calibrators. The  $1\sigma$  scatter decreases with increasing effective wavelength, dropping from from 0.39 to 0.20 dex. The solid green lines represent the MIRI calibrations of Battisti et al. (2015), where we have segmented the line so that it covers only the relevant SFR range, and extrapolated the line so that it covers the SFR of our galaxies (dotted green line).

Using the less conservative Kewley et al. (2001) BPT criteria, and after the removal of known AGN (such as IC 5298, NGC 1614, NGC 3079, and NGC 5033 etc.) and extreme

outliers, we find normalizations and indices agree to within 0.13 dex and 0.02 of the power-law fits that we previously determined using Kauffmann et al. (2003) BPT selection

criteria. We thus conclude that our calibrations have a weak dependence on the chosen BPT criterion, with SFRs decreasing by  $\sim 20\%$  (at fixed MIR luminosity) if we replace the Kauffmann et al. (2003) criterion with the Kewley et al. (2001) criterion.

Figure 4 and Table 1 illustrate that the  $1\sigma$  scatter of the data about the power-law fits decreases with increasing wavelength from 0.38 dex for F560W to 0.20 dex for F2550W. This scatter is comparable to the scatter that we measure for the *Spitzer* and *WISE* filters, as well as the scatter measured by Brown et al. (2017) and Cluver et al. (2017) for filters of comparable wavelengths. The scatter is high in the shorter-wavelength filters due to silicate absorption and peaks in PAH emission, including strong features at  $7.7\ \mu\text{m}$  and  $\sim 12\ \mu\text{m}$  (e.g., Brandl et al. 2006; Cluver et al. 2014). Longer wavelengths are dominated by blackbody radiation from warm dust, resulting in less scatter.

While the scatter generally decreases with increasing wavelength, the F1000W filter has a relatively low scatter of 0.24 dex, which is significantly less than filters with comparable effective wavelengths. This may be due to  $10\ \mu\text{m}$  being in the sweet spot where PAH emission is canceled out by silicate absorption.

Brown et al. (2017) SFR calibrations included a number of dwarf galaxies with *Spitzer* and *WISE* photometry but no *Spitzer* IRS spectroscopy. That said, we observe scatter that is comparable to Brown et al. (2017) for the relevant wavelengths, even though we have used higher-luminosity galaxies to calibrate the MIRI filters as SFR indicators. Our best fits have comparable normalization and power-law indices as the relevant Brown et al. (2017) fits (when applicable), so extrapolations of our relations should apply to dwarf galaxies. We conclude that the longer wavelength *JWST* MIRI filters, along with the F1000W filter, will provide the most accurate SFR measurements.

In Figure 4 there are several low-luminosity outliers (e.g., UGCA 166 and Mrk 475) and these are also seen in the Brown et al. (2017) calibrations. Lower-luminosity galaxies used for the Brown et al. (2017) calibrations do fall along their power-law relations, so we do not believe the outliers in Figure 4 imply a breakdown of the overall power-law relation. As noted earlier, we were unable to include the lowest-luminosity galaxies from Brown et al. (2017) in our calibrations as they lack *Spitzer* IRS spectroscopy.

Our calibrations can be directly compared to those of Battisti et al. (2015), who presented calibrations of SFR indicators in  $6\text{--}70\ \mu\text{m}$  wavelength range, including calibrations of six MIRI filters, some of which are plotted in Figure 4. To compare our calibrations with those of Battisti et al. (2015) we use their conversion factors that correspond to  $z = 0$ . Our sample includes relatively low-luminosity galaxies, whereas the Battisti et al. (2015) sample is focused on galaxies with SFRs of  $\sim 1\text{--}10\ M_{\odot}\ \text{yr}^{-1}$  with a few galaxies with SFRs  $> 10\ M_{\odot}\ \text{yr}^{-1}$ . Battisti et al. (2015) have assumed that SFR is directly proportional to MIR luminosity, with a conversion factor that is determined via fits of synthetic observations of a redshifted composite spectrum. While this assumption may be correct for galaxies with high luminosity, we find that the relationship between  $H\alpha$  luminosity and SFR is a power law. This can be clearly seen in Figure 4, where our relationship and that of Battisti et al. (2015) intercept at

higher luminosities, while at lower  $H\alpha$  luminosities the relationships from Battisti et al. (2015) are  $\approx 1$  dex higher in MIR luminosity than our calibrations. From this we conclude that the calibrations from Battisti et al. (2015) will provide an accurate SFR measurement for higher-luminosity galaxies; however, our calibrations are more accurate for lower-luminosity galaxies (i.e., dwarf galaxies). An obvious extension to our work will be to calibrate the *JWST* MIRI filters for a wider luminosity range, including high-luminosity galaxies that fall in the range where prior calibrations have adopted a one-to-one relationship between MIR luminosity and SFR.

## 5. Summary

We have calibrated the *JWST*, *Spitzer*, and *WISE* MIR filters as SFR indicators using photometry synthesized from *Spitzer* spectra and Balmer-decrement-corrected  $H\alpha$  luminosities, measured with scanned long-slit spectroscopy (Moustakas & Kennicutt 2006; Moustakas et al. 2010; Brown et al. 2014, 2017). Our galaxy sample covers a wide range of luminosities and thus our calibrations extend to lower luminosities than other studies such as Battisti et al. (2015). We verified our approach by comparing our *Spitzer* and *WISE* calibrations with those from the literature.

For *Spitzer*, *WISE*, and *JWST* we find galaxies with an  $H\alpha$  luminosity of  $10^{40}\ \text{erg s}^{-1}$ , the corresponding MIR  $\nu L_{\nu}$  is between  $10^{40.49}$  and  $10^{41.37}\ \text{erg s}^{-1}$ . We find that the relationship between luminosity in MIR filters is approximated by power laws with indices between 1.17 and 1.32. For the MIRI filters, the  $1\sigma$  scatter of the data about our power-law fits is between 0.39 and 0.20 dex, which are comparable to the scatter measured by Brown et al. (2017) for equivalent wavelength filters. This scatter decreases with increasing wavelength as PAHs emission and silicate absorption dominate at shorter wavelengths, whereas longer wavelengths are dominated by blackbody radiation from dust. The exception to this is the  $10\ \mu\text{m}$  filter (F1000W) which has a scatter of just 0.24 dex; this is significantly less than other *JWST* filters with comparable effective wavelengths.

This Letter is based in part on archival data obtained with the *Spitzer Space Telescope*, which is operated by the Jet Propulsion Laboratory, California Institute of Technology under a contract with National Aeronautics and Space Administration. Support for this Letter was provided by an award issued by JPL/Caltech. This publication makes use of data products from the Wide-field Infrared Survey Explorer, which is a joint project of the University of California, Los Angeles, and the Jet Propulsion Laboratory/California Institute of Technology, funded by the National Aeronautics and Space Administration. This research is based on observations with AKARI, a JAXA project with the participation of ESA.

*Facilities:* Bok, *JWST*, *Spitzer*, *WISE*, *Akari*.


## ORCID iDs

Madhooshi R. Senarath  <https://orcid.org/0000-0003-1905-5426>

Michael J. I. Brown  <https://orcid.org/0000-0002-1207-9137>

Michelle E. Cluver  <https://orcid.org/0000-0002-9871-6490>

Lee Armus  <https://orcid.org/0000-0003-3498-2973>

Thomas H. Jarrett  <https://orcid.org/0000-0002-4939-734X>

## References

- Baldwin, J. A., Phillips, M. M., & Terlevich, R. 1981, *PASP*, 93, 5
- Battisti, A. J., Calzetti, D., Johnson, B. D., & Elbaz, D. 2015, *ApJ*, 800, 143
- Bonvin, V., Courbin, F., Suyu, S. H., et al. 2017, *MNRAS*, 465, 4914
- Bouchet, P., Garcia-Marin, M., Lagage, P.-O., et al. 2015, *PASP*, 127, 612
- Brandl, B. R., Bernard-Salas, J., Spoon, H. W. W., et al. 2006, *ApJ*, 653, 1129
- Brown, M. J. I., Moustakas, J., Kennicutt, R. C., et al. 2017, *ApJ*, 847, 136
- Brown, M. J. I., Moustakas, J., Smith, J.-D. T., et al. 2014, *ApJS*, 212, 18
- Calzetti, D., Armus, L., Bohlin, R. C., et al. 2000, *ApJ*, 533, 682
- Calzetti, D., Wu, S.-Y., Hong, S., et al. 2010, *ApJ*, 714, 1256
- Cappellari, M., & Emsellem, E. 2004, *PASP*, 116, 138
- Cardelli, J. A., Clayton, G. C., & Mathis, J. S. 1989, *ApJ*, 345, 245
- Chabrier, G. 2003, *PASP*, 115, 763
- Cluver, M. E., Jarrett, T. H., Dale, D. A., et al. 2017, *ApJ*, 850, 68
- Cluver, M. E., Jarrett, T. H., Hopkins, A. M., et al. 2014, *ApJ*, 782, 90
- Davies, L. J. M., Robotham, A. S. G., Driver, S. P., et al. 2015, *MNRAS*, 452, 616
- Falcon-Barroso, J., Bacon, R., Bureau, M., et al. 2006, *MNRAS*, 369, 529
- Glasse, A., Rieke, G. H., Bauwens, E., et al. 2015, *PASP*, 127, 686
- Greene, T. P., Kelly, D. M., Stansberry, J., et al. 2017, *JATIS*, 3, 035001
- Hogg, D. W., Baldry, I. K., Blanton, M. R., & Eisenstein, D. J. 2002, arXiv: astro-ph/0210394
- Jarrett, T. H., Cohen, M., Masci, F., et al. 2011, *ApJ*, 735, 112
- Jarrett, T. H., Masci, F., Tsai, C. W., et al. 2013, *ApJ*, 145, 6
- Jaskot, A. E., Oey, M. S., Salzer, J. J., et al. 2015, *ApJ*, 808, 66
- Kauffmann, G., Heckman, T. M., White, S. D. M., et al. 2003, *MNRAS*, 341, 33
- Kennicutt, R. C. 1998, *ARA&A*, 36, 189
- Kennicutt, R. C., & Evans, N. J. 2012, *ARA&A*, 50, 531
- Kennicutt, R. C., Jr., Hao, C.-N., et al. 2009, *ApJ*, 703, 1672
- Kewley, L. J., Dopita, M. A., Sutherland, R. S., et al. 2001, *ApJ*, 556, 121
- Kroupa, P. 2001, *MNRAS*, 322, 231
- Lee, J. C., Hwang, H. S., & Ko, J. 2013, *ApJ*, 774, 62
- Moustakas, J., & Kennicutt, R. C., Jr. 2006, *ApJS*, 164, 81
- Moustakas, J., Kennicutt, R. C., Jr., Tremonti, C. A., et al. 2010, *ApJS*, 190, 233
- Osterbrock, D. E. 1989, *Astrophysics of Gaseous Nebulae and Active Galactic Nuclei* (Mill Valley, CA: Univ. Science Books)
- Salpeter, E. E. 1955, *ApJ*, 121, 161
- Sarzi, M., Falcón-Barroso, J., Davies, R. L., et al. 2006, *MNRAS*, 366, 1151
- Wu, H., Cao, C., Hao, C.-N., et al. 2005, *ApJL*, 632, L79
- Wu, J., Evans, N. J., II, Gao, Y., et al. 2005, *ApJ*, 635, 173
- Zhu, Y.-N., Wu, H., Cao, C., & Li, H.-N. 2008, *ApJ*, 686, 155